Article

Synergistic Lubricating Performance of Graphene Oxide and Modified Biodiesel Soot as Water Additives

Chuan Li [1,†], Bo Wu [2,*,†], Xiaoju Chen [1], Lei Li [1], Xinyun Wang [1], Xiaobao Gao [1], Xiaodong Wang [1], Kunhong Hu [3] and Xianguo Hu [4,*]

1   School of Chemistry and Material Engineering, Chaohu University, Hefei 238000, China
2   School of Pharmacy, Anhui University of Chinese Medicine, Hefei 230012, China
3   Department of Energy Materials and Chemical Engineering, Hefei University, Hefei 230601, China
4   School of Mechanical Engineering, Hefei University of Technology, Hefei 230009, China
*   Correspondence: wubo@ahtcm.edu.cn (B.W.); xghu@hfut.edu.cn (X.H.)
†   These authors contributed equally to this work.

Abstract: The tribological performance of graphene oxide (GO) nanosheets, modified biodiesel soot (MBS) nanoparticles, and their mixture (MBS–GO) nanoparticles as lubricant additives in water was evaluated using a reciprocating ball-on-plate tribometer. The effects of different mass ratios of GO to MBS, additive concentrations, and loads, as well as corresponding lubrication mechanisms, were studied. The tribological measurements showed that the water-containing 0.5 wt% additives at a mass ratio of 60:40 (GO to MBS) resulted in larger reductions in friction coefficient (69.7%) and wear volume (60.5%) than water. Owing to the synergistic effect of GO nanosheets and MBS nanoparticles, the MBS–GO aqueous sample showed superior lubricating properties compared to water as well as GO and MBS aqueous samples. The good tribological properties of MBS–GO nanoparticles in water are attributed to the formation of a tribofilm of hybrid nanoparticles that effectively protects the friction interface. Moreover, the MBS nanoparticles can provide lubrication by acting as ball bearings.

Keywords: graphene oxide; biodiesel soot; lubricant additive; water; nanoparticles

1. Introduction

Friction, wear, and lubrication are constant problems in the various engineering fields of industrial production [1]. Lubricants are critical for reducing friction, wear, and energy consumption as well as prolonging the service life of mechanical equipment [2]. Conventional oil-based lubricants are still dominant in today's market; however, their environmental impacts cannot be ignored [3]. Recently, environment friendly water-based lubricants have been used in many fields, particularly in specialized engineering fields, such as underwater robots, ships, and biological systems [4,5]. As a result, water-based lubricants are an important development direction of lubricants. Good lubricating additives are the key to produce water-based lubricants with excellent antifriction properties and wear resistance [6].

Carbon nanomaterials have recently attracted extensive attention for use as lubricating additives in water [7]. Some carbon nanomaterials, such as carbon quantum dots, onion-like carbon, graphene, nanodiamonds, and carbon nanotubes, have been explored for the development of water-based lubricating additives owing to their unique physical and chemical properties [8–11]. Graphene oxide (GO) has a unique crystal structure and self-lubricating properties [12,13]. Thus, it has become a research hotspot as a water-based lubricating additive. Su et al. [14] and Zhang et al. [15] found that GO as an additive in water show antifriction and antiwear effects as they can adsorb onto the friction plate to form a tribofilm. Gan et al. [16] prepared GO with a high degree of exfoliation (GO-EmimN(CN)$_2$) using EmimN(CN)$_2$ as an intercalator. The GO-EmimN(CN)$_2$ showed high lubrication due to the presence of multiple self-lubricating films including easily sheared

deposition films. Gan et al. [17] reported that GO has a self-healing function in the friction process, thus reducing the wear of friction pairs. Min et al. [18] prepared fluorinated GO (FGO) with abundant oxygen-containing functional groups via a hydrothermal method using HF and HNO_3; 0.7 wt% FGO showed good antifriction and antiwear effects in water owing to the formation of a transfer film formed on the friction surface. Wu et al. [19] investigated the tribological properties of GO in bio-oil and found that a high GO content leads to adhesive wear. However, an appropriate amount of GO in water could form a complete lubricating film on the friction surface and provide a good lubricating effect. Thus, GO deposited on the contact surface as a nanosheet could protect the friction interface by forming an effective lubricating film.

It is well known that different types of nanoparticles show unique advantages when mixed in lubricants because of their synergistic tribological behaviors. Wu et al. [20] found that using GO and nanodiamonds as lubricant additives in water produced lower friction coefficients and wear volumes than those achieved using pure GO and nanodiamond solutions. Huang et al. [21] found that a GO–alumina lubricant showed good wear resistance and reduced friction via a synergistic lubricating effect. Du et al. [22] studied the tribological properties of TiO_2-modified GO as a lubricating water additive. The addition of TiO_2-modified GO to water significantly improved the friction reduction and wear resistance. Min et al. [23] investigated the tribological behaviors of GO/carboxyl-functionalized multiwalled carbon nanotube hybrids and found that the hybrids possessed good antiwear and friction-reducing properties. Guo et al. [24] synthesized aminated silica-modified GO and used it as a water additive, which dramatically improved the lubricating performance of water, even under high contact pressure. The abovementioned research shows that the use of appropriate nanoparticles with GO can achieve improved antifriction and antiwear properties.

Soot is formed during the incomplete fuel combustion in diesel engines or gasoline direct-injection engines. Vehicles exhaust soot into the atmosphere through gaseous emissions, severely harming the human health and atmosphere [25,26]. In addition, soot is a carbon nanomaterial with approximately 30–50-nm-sized spherical particles [27,28]. Recently, soot has been used to convert contaminants into useful materials [29–31]. Li et al. [32,33] found that biodiesel soot could be uniformly dispersed in water through thermal oxidation or nitric acid treatment method. The antifriction and antiwear performance of water was improved by adding the treated soot. Thus, soot has potential applications as an additive for water-based lubricants. The research to date mainly focuses on the tribological performance of spherical soot particles blended with lubricants. However, few studies investigated the performance of different types of soot–nanomaterial hybrids in water as lubricating additives.

The prospect of using layered and spherical nanomaterials as lubricating additives is enticing due to their potential synergistic effect [34,35]. To meet the needs of different industrial applications, it is necessary to study different steel materials as the friction pairs. Several studies have investigated the friction and wear behaviors of water-based lubricants containing nanomaterials additives with GCr15 steel/stainless steel frictional pairs under different frictional conditions and found that nanomaterial additives have good lubricating effects [36–38]. Based on the considerations mentioned in previous paragraphs, the tribological properties of GO, modified biodiesel soot (MBS) and their mixture (MBS–GO) in water were respectively tested using a ball-on-plate tribometer for GCr15 steel/304 austenitic stainless steel contact in this study. The effects of different mass ratios of GO to MBS, additive concentrations, and loads were discussed along with the corresponding mechanisms. We demonstrate by comparison that the addition of MBS–GO improves the friction reduction and wear resistance of water via its synergistic effect.

2. Materials and Methods

2.1. Materials

GO nanosheets were supplied by Nanjing XFNANO Materials Tech Co., Ltd. (Nanjing, China). From biodiesel soot, MBS nanoparticles were prepared using a nitric acid treatment method [28,32]. The details of the biodiesel soot collection and MBS nanoparticle preparation are presented in our previous report [39]. Ultrapure water was produced by a UPT-11-10T water purification system (Sichuan ULUPRE Technology Co., Ltd., Chengdu, China) and was used in all the experiments.

The detailed processes of MBS–GO aqueous sample preparation are as follows: GO and MBS with different mass ratios (100:0, 80:20, 60:40, 50:50, 40:60, 20:80, and 0:100) were mixed in water. The total additive concentration in water is 0.5 wt%. The mixtures were first stirred with a glass rod for 10 min and then magnetically stirred for 20 min. Finally, the mixtures were ultrasonicated for 30 min to achieve a homogeneous dispersion. After experimentally obtaining the best mass ratio, the MBS–GO aqueous samples with different additive concentrations of 1, 0.5, 0.25, and 0.125 wt% were prepared by gradient dilution. The same procedure was performed to disperse the additives in water.

2.2. Tribological Tests

The tribological tests were performed on an HSR-2M reciprocating ball-on-plate tribometer (Lanzhou Zhongkekaihua Technology Development Co., Ltd., Lanzhou, China) at room-temperature. A schematic of the tribological test is shown in Figure 1. The upper ball (6-mm diameter) used for the tribological tests was made of GCr15 steel with a hardness of 647–861 HV. The lower plate was made of 304 austenitic stainless steel with dimensions of 60 mm × 30 mm × 5 mm and a hardness of 200–210 HV. The surface roughness was maintained at 0.02 μm for all upper balls and lower plates. Before the tribological tests, the upper balls and lower plates were cleaned ultrasonically with ethanol for 10 min. The friction tests were performed at an average sliding speed of 50 mm/s, a stroke length of 5 mm, an oscillating frequency of 5 Hz, and different loads of 10–40 N for 30 min. The friction coefficients were recorded using the software attached to the tribometer. The average friction coefficient was calculated from the average value of friction coefficient over the 30 min testing time. After the friction tests, the friction pairs were ultrasonically cleaned with ethanol and then dried using a hair dryer. The wear volume of the lower plate was measured and calculated using three-dimensional (3D) laser-scanning microscope (VK-X100, Keyence, Osaka, Japan). Experiments were repeated at least three times under each condition.
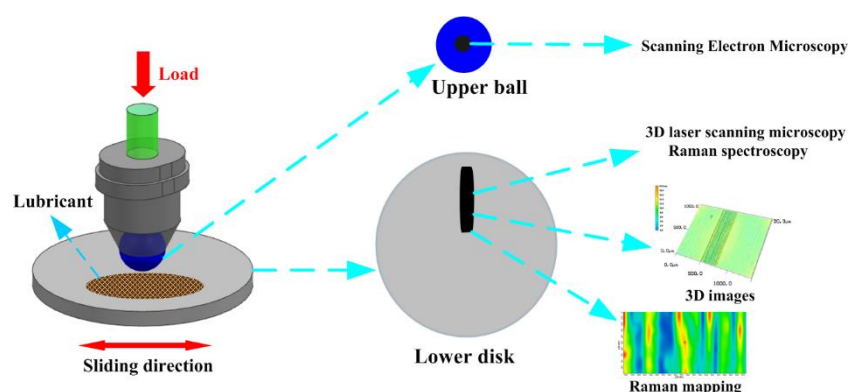

Figure 1. Schematic of the tribological tests and analysis measure methods.

The Hertz contact diameter (*a*) and contact stress (*P*) of the ball-on-plate contact were calculated using the Hertz's theory [40]:

$$a = 2 \times \left(\frac{2}{3} \times \frac{W \times R}{E\prime} \right)^{\frac{1}{3}} \tag{1}$$

$$P = \frac{4 \times W}{\pi \times a^2} \tag{2}$$

where W is the normal load (10, 20, and 40 N), R is the equivalent radius of curvature (3×10^{-3} m), and E' is the effective elastic modulus (2.33×10^{11} Pa). Under different normal loads, the Hertz diameters were 8.82×10^{-5}, 1.11×10^{-4}, and 1.40×10^{-4} m, respectively, and the contact stresses were 1.64×10^9, 2.06×10^9, and 2.60×10^9 Pa, respectively.

The Lambda ratio (λ) was determined using the Dowson and Hamrock's minimum film thickness formula [41,42]:

$$h_{\min} = 3.63 \times R \times \frac{(\alpha \times E')^{0.49} \times \left(\frac{\eta_0 \times U}{E' \times R}\right)^{0.68}}{\left(\frac{W}{E' \times R^2}\right)^{0.073}} \left(1 - e^{-0.68k}\right) \tag{3}$$

$$\lambda = \frac{h_{\min}}{\sqrt{Ra_1^2 + Ra_2^2}} \tag{4}$$

where R is the equivalent radius of curvature (3 mm), k is the elliptical parameter (~1), η_0 is the dynamic viscosity of water (1×10^{-3} Ns/m^2), α is the pressure–viscosity coefficient of water (2.2×10^{-8} m^2/N), U is the sliding speed (0.05 m/s), and R_{a1} and R_{a2} are the surface roughness of the ball and plate, respectively ($R_{a1} = R_{a2} = 0.02$ µm). The maximum value of λ (for $W = 10$ N) obtained is 0.035, suggesting that the friction tests were performed in the boundary-lubrication regime.

2.3. Analysis Methods

The morphologies of the MBS nanoparticles, GO nanosheets, and MBS–GO nanoparticles were determined by a JEM-2100F field-emission transmission electron microscope (FETEM, JEOL, Tokyo, Japan). The structural information of the nanoparticles samples was characterized using a DXR2 micro-Raman spectroscope (ThermoFisher Scientific, Waltham, MA, USA). The particle size distributions in water were analyzed using a Nano-ZS90 zeta potentiometer (Malvern, Worcestershire, UK). Additionally, Figure 1 shows methods used for analyzing wear traces. Surface micrographs and elemental maps of wear traces of upper balls after tribological testing were determined using a SU8010 field-emission scanning electron microscope (FESEM, Hitachi, Tokyo, Japan) equipped with energy dispersive spectrometer (EDS). EDS applied an acquisition voltage of 20 kV. The 3D micrographs and profile curves of the wear traces of lower plates after tribological tests were obtained using a VK-X100 3D laser-scanning microscope (Keyence, Osaka, Japan). Raman mappings of the wear traces of lower plates after tribological tests were determined by micro-Raman spectroscopy.

3. Results and Discussion

3.1. Characterizations

The FETEM characterization results of the MBS nanoparticles, GO nanosheets, and MBS–GO nanoparticles are illustrated in Figure 2. As shown in Figure 2a, the MBS nanoparticles are spherical with diameters of approximately 40 nm. The MBS nanoparticles display an agglomeration phenomenon, wherein many primary particles formed chain-like conglomerates [43,44]. As shown in Figure 2b, the GO nanosheets have a typical layered structure with wrinkles. The representative FETEM images of the MBS–GO nanoparticles are shown in Figure 2c,d. The MBS nanoparticles adhered to the GO nanosheets, which reduced the agglomeration of MBS nanoparticles and could improve lubrication [21,45].
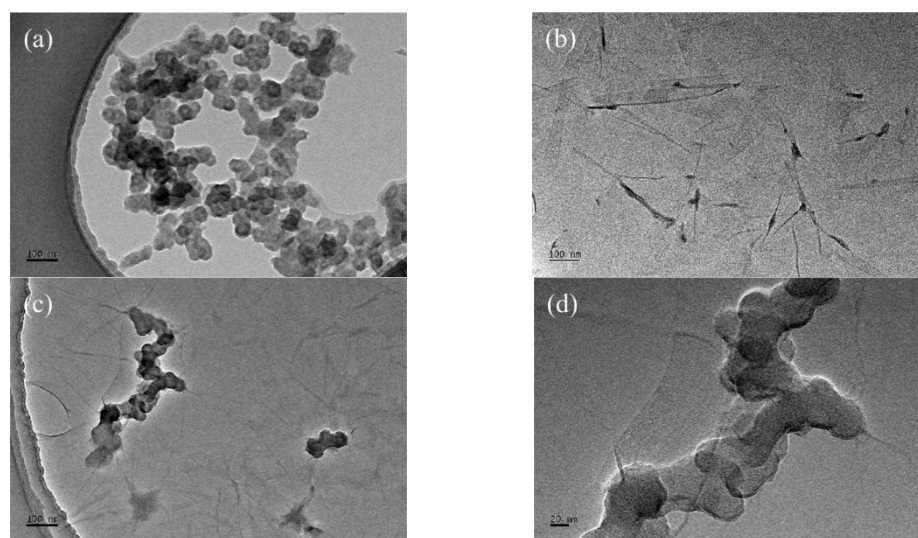
Figure 2. FETEM images of the (**a**) MBS nanoparticles, (**b**) GO nanosheets, and (**c**,**d**) MBS–GO nanoparticles.

The particle size distributions of the GO nanosheets, MBS nanoparticles, and MBS–GO nanoparticles in water are shown in Figure 3. The GO nanosheets, MBS nanoparticles, and MBS–GO nanoparticles in water comprise particles ranging from tens to hundreds of nanometers. The results show that the GO nanosheets, MBS nanoparticles, and MBS–GO nanoparticles can be dispersed in water and that the preparation of MBS–GO aqueous samples has no effect on the particle size distribution and structure.
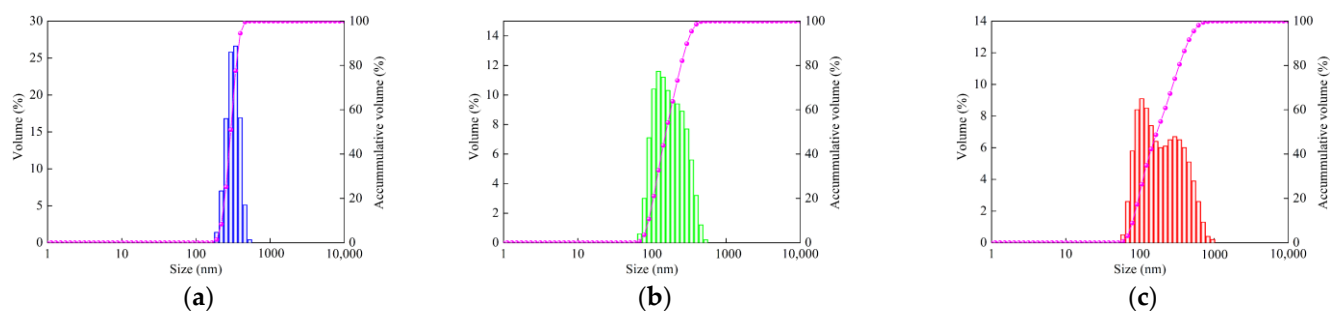

Figure 3. Particle size distributions of the (**a**) GO nanosheets, (**b**) MBS nanoparticles, and (**c**) MBS–GO nanoparticles.

The Raman spectra of the GO nanosheets, MBS nanoparticles, and MBS–GO nanoparticles are shown in Figure 4. A typical Raman spectrum of graphite has intense G and D bands located at 1580 and 1350 cm^{-1}, respectively, ascribed to the first order of E_{2g}-mode scattering and the vibration of sp^3 carbon atoms with dangling bonds in the termination plane of disordered graphite [46,47]. In the spectrum of the GO nanosheets, the peaks corresponding to the D and G bands are located at 1352 and 1590 cm^{-1}, respectively. The oxygenation of graphite causes a shift in the G band [14]. The spectrum of the MBS nanoparticles exhibits the D- and G-band peaks at 1350 and 1587 cm^{-1}. The large size of and defects in the MBS nanoparticles contribute to the upshift of the G band [48]. The spectrum of the MBS–GO nanoparticles shows two peaks centered at 1350 and 1588 cm^{-1} corresponding to the D and G bands, respectively. The shift in the G band might be related to the defects on the surfaces of the MBS–GO nanoparticles. These results show that no obvious changes occurred in the chemical structure of the MBS–GO aqueous sample during its preparation. This conclusion is consistent with the results of the particle size distributions.
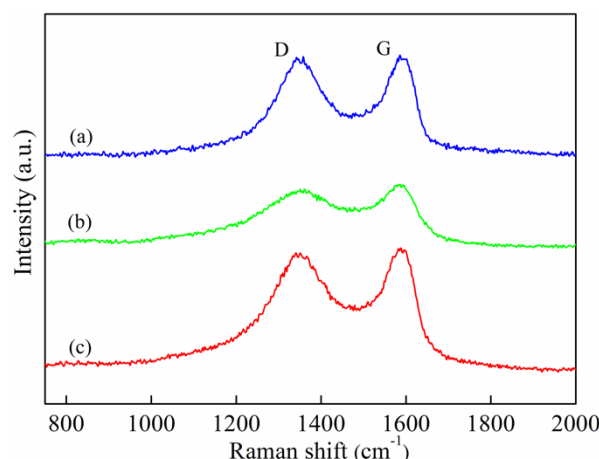
Figure 4. Raman analysis of the (**a**) GO nanosheets, (**b**) MBS nanoparticles, and (**c**) MBS–GO nanoparticles.

Figure 5 shows the digital images of the water-containing 0.5 wt% MBS−GO nanoparticles with a GO−to−MBS mass ratio of 60:40 at 0 and 12 h after sonication. A uniform suspension was obtained after 30 min of ultrasonic treatment. Moreover, no sedimentation was observed in the MBS–GO aqueous sample after 12 h. The dispersion results indicated that the stable suspension time is longer than the 30 min required for the friction experiment. The MBS–GO nanoparticles have good dispersion stability in water.
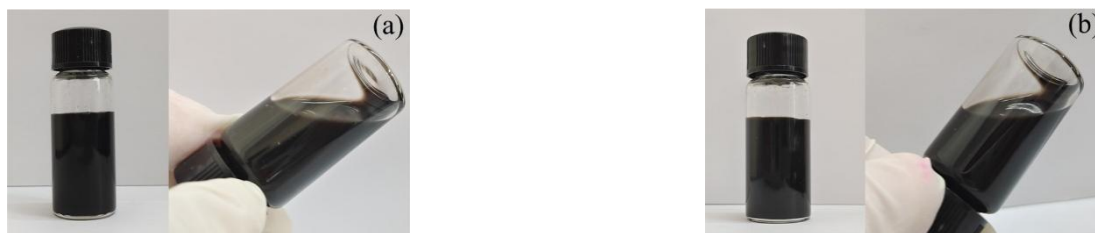

Figure 5. Digital images of the MBS–GO aqueous sample (**a**) 0 and (**b**) 12 h after sonication.

3.2. Antiwear and Friction Reduction

The variations in the average friction coefficient and wear volume of the MBS–GO nanoparticles with different GO−to−MBS mass ratios (mass ratio: 100:0, 80:20, 60:40, 50:50, 40:60, 20:80, and 0:100; additive content = 0.5 wt%; testing time = 30 min; applied load = 10 N; and speed = 50 mm/s) are shown in Figure 6. The average friction coefficient and wear volume for water are 0.725 and 7.59×10^6 μm^3, respectively; these are the highest values among the eight lubricant samples tested. When the GO nanosheets or MBS nanoparticles are added separately, the average friction coefficients and wear volumes of the both are lesser than those of water are. This shows that the introduction of the GO nanosheets or MBS nanoparticles to water effectively enhances the antifriction and antiwear properties of water [33,49]. Additionally, the average friction coefficient and wear volume after lubricating with the MBS–GO nanoparticles in water were lower than after lubricating with either GO nanosheets or MBS nanoparticles in water. For the MBS–GO nanoparticles, the average friction coefficient and wear volume decreased with decreasing GO content until a mass ratio of 60:40 (GO:MBS) was achieved. This may be attributed to the ability of the GO nanosheets to deposit on the friction interface as a carbon film. Meanwhile, due to the addition of the MBS nanoparticles, they also enter the friction region and provide lubrication. The lowest average friction coefficient and wear volume were found at a mass ratio of 60:40 (GO:MBS), which reduced the friction coefficient (0.220) and wear volume (3.00×10^6 μm^3) from those of water by 69.7% and 60.5%, respectively. With further decreases in the GO−to−MBS mass ratio, the average friction coefficient and wear volume increased to varying extents. Thus, the MBS–GO nanoparticles showed

better lubricating performance than the constituting components (GO nanosheets or MBS nanoparticles), and the optimal GO−to−MBS mass ratio was 60:40.
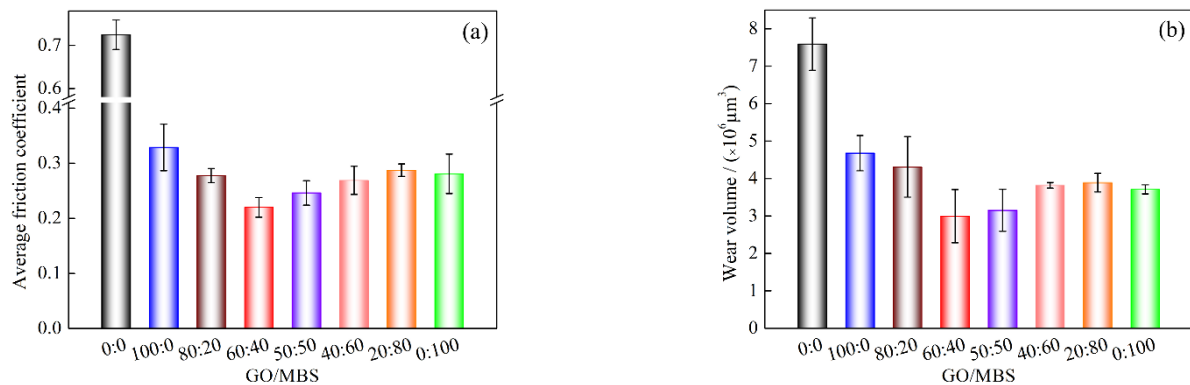

Figure 6. Influence of mass ratio of GO to MBS on (**a**) antifriction and (**b**) antiwear properties (additive content = 0.5 wt%, load = 10 N, speed = 50 mm/s, testing time = 30 min).

The variations in the average friction coefficient and wear volume with different concentrations of the GO nanosheets, MBS nanoparticles, and MBS–GO nanoparticles (mass ratio = 60:40; concentration of the MBS–GO nanoparticles = 1, 0.5, 0.25, and 0.125 wt%; testing time = 30 min; applied load = 10 N; and speed = 50 mm/s) are illustrated in Figure 7. The average friction coefficient and wear volume decreased with increasing concentration of additives when the concentration was <0.5 wt%, except for a slight increase in the wear volume of GO at 0.25 and 0.5 wt% concentrations. The results indicated that the additive concentration is important for enhancing the antifriction and antiwear properties of the aqueous samples. As the concentration was increased beyond 0.5 wt%, the average friction coefficient and wear volume increased with increasing additive concentrations because the agglomerated nanoparticles, originating from the high concentration of nanoparticles in water, caused abrasive wear [45]. The minimum average friction coefficient and wear volume were obtained using 0.5 wt% MBS–GO nanoparticles. Therefore, 0.5 wt% was chosen as the optimal concentration of these lubricant additives in water. Notably, the MBS–GO aqueous sample had the lowest average friction coefficient and wear volume among the three lubricant samples at all test concentrations. This result indicated that the MBS–GO aqueous sample had better lubrication properties than the other two lubricant samples, confirming the synergistic lubrication effects of the MBS nanoparticles and GO nanosheets dispersed in water.
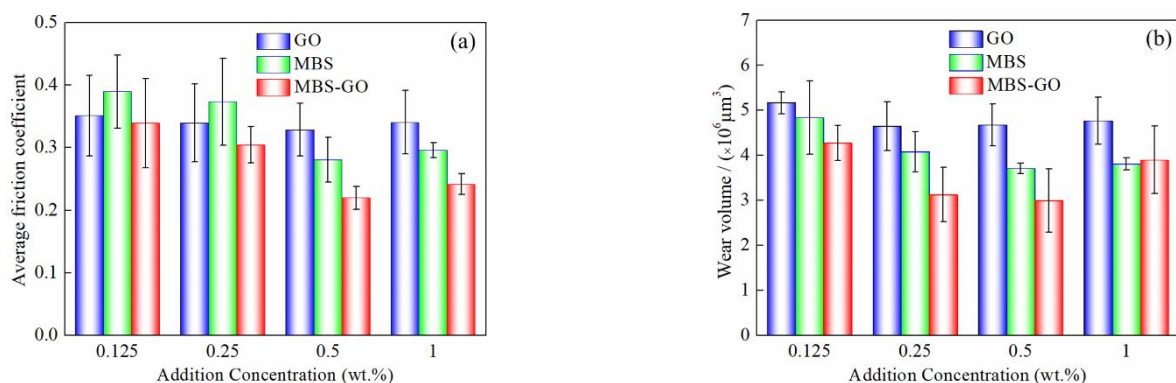

Figure 7. Influence of the concentration of the GO nanosheets, MBS nanoparticles, and MBS–GO nanoparticles on (**a**) antifriction and (**b**) antiwear properties (GO−to−MBS mass ratio = 60:40, load = 10 N, speed = 50 mm/s, and testing time = 30 min).

The variations in the average friction coefficient and wear volume with applied load (mass ratio: 60:40; additive content: 0.5 wt%; testing time: 30 min; applied load: 10, 20, and 40 N; and speed: 50 mm/s) are shown in Figure 8. It was evident that the average friction coefficients of water as well as GO, MBS, and MBS–GO aqueous samples decreased with increasing tested load. Each of the three aqueous samples reduces the average friction coefficient of water under the tested load. The MBS–GO aqueous sample has a friction coefficient smaller than that of the GO and MBS aqueous samples as well as water. Interestingly, the wear volume of all four samples increased with increasing load, suggesting that all three aqueous samples could reduce the wear volume. The wear volume of the MBS–GO aqueous sample was lower than the GO and MBS aqueous samples as well as water. The results showed that the GO nanosheets, MBS nanoparticles, MBS–GO nanoparticles actively form a tribofilm under each load. Moreover, the MBS–GO aqueous sample showed the best tribological performance, which could be attributed to the GO nanosheets and MBS nanoparticles participating in the friction between the ball–plate friction pairs, creating a synergistic effect [20,50].
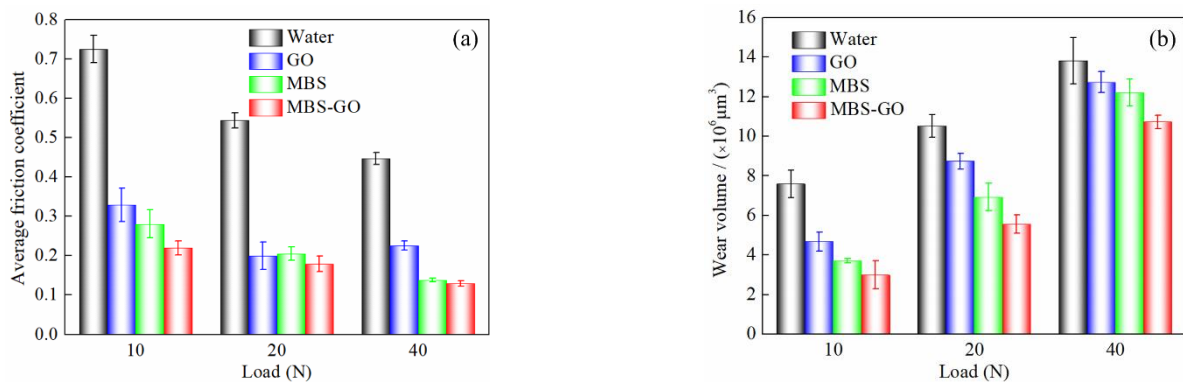

Figure 8. Influence of load on (**a**) antifriction and (**b**) antiwear properties (GO−to−MBS mass ratio = 60:40, speed = 50 mm/s, testing time = 30 min, and additive content = 0.5 wt%).

3.3. Worn Surface Analysis

Figure 9 shows the 3D micrographs and profile curves of the wear traces of the lower plates lubricated with water as well as GO, MBS, and MBS–GO aqueous samples at an additive content of 0.5 wt%, a mass ratio of 60:40, a load of 10 N, a speed of 50 mm/s, and a testing time of 30 min. The profile curves of and wear area on the lower plates were obtained using the VK Analyzer to calculate 200 cross sections from the middle of the wear traces. Based on the 3D micrographs and profile curves of the wear traces of the lower plates, those lubricated by water underwent the most severe wear, showing the poorest wear resistance, and had a wear area of 1658.05 μm^2. It is clear that the addition of 0.5 wt% GO nanosheets or MBS nanoparticles decreased the wear area to 1028.17 and 765.96 μm^2, respectively. This is because the GO nanosheets and MBS nanoparticles deposit on the sliding contact zone and generate a tribofilm, which plays an important role in improving the antiwear performance of water. As expected, the addition of the MBS–GO nanoparticles to water resulted in a significant reduction in deep and wide grooves, with a wear area of 457.28 μm^2. The above results confirm that the MBS–GO nanoparticles could better improve the antiwear performance of water than the GO nanosheets or MBS nanoparticles alone [51].
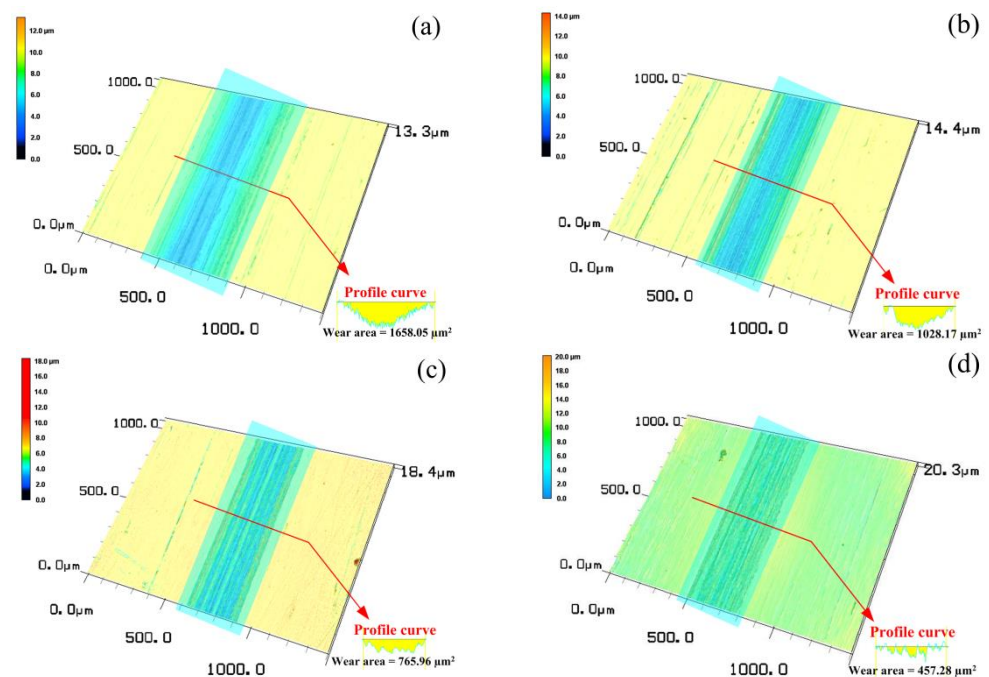
Figure 9. 3D micrographs and profile curves of wear traces of lower plates after tribological test for the (**a**) water sample, (**b**) GO aqueous sample, (**c**) MBS aqueous sample, and (**d**) MBS–GO aqueous sample (additive content = 0.5 wt%, GO−to−MBS mass ratio = 60:40, load = 10 N, speed = 50 mm/s, and testing time = 30 min).

The surface micrographs and EDS elemental maps of the wear traces of upper balls lubricated with water as well as GO, MBS, and MBS–GO aqueous samples (additive content: 0.5 wt%, mass ratio = 60:40, load: 10 N, speed: 50 mm/s, and testing time: 30 min) are shown in Figure 10. The surface micrographs and EDS elemental maps are obtained from the center of the wear traces of the upper balls. Figure 10a shows severe wear of the surface lubricated with water, which has many wide grooves, suggesting abrasive wear [52,53]. There are some wide grooves on the worn surface lubricated with the GO aqueous sample (Figure 10b). Meanwhile, patches formed on the partially worn surface with smaller grooves than those on the surface lubricated with water are seen. This can be attributed to the protective graphene tribofilm present on the friction surface [54]. As shown in Figure 10c, the grooves were narrower and shallower on the worn surface lubricated MBS aqueous sample than with water, which can be attributed to the MBS serving as a ball bearing during sliding [55]. As shown in Figure 10d, the addition of the MBS–GO nanoparticles to the water yielded better antiwear performance with smaller grooves than those found on the surfaces lubricated with the individual aqueous sample additives. This may be due to the GO layers and spherical MBS nanoparticles forming hybrid nanoparticles that combined the advantages of both additives and effectively enhanced the wear resistance and reduced the friction [21,51]. These results are consistent with the results shown in Figure 9. Additionally, the C content on the worn surfaces lubricated with the GO, MBS, and MBS–GO aqueous samples increased compared to that lubricated with water. This confirmed that carbon films are deposited on the surfaces of the friction pairs because of the nanomaterial additions.
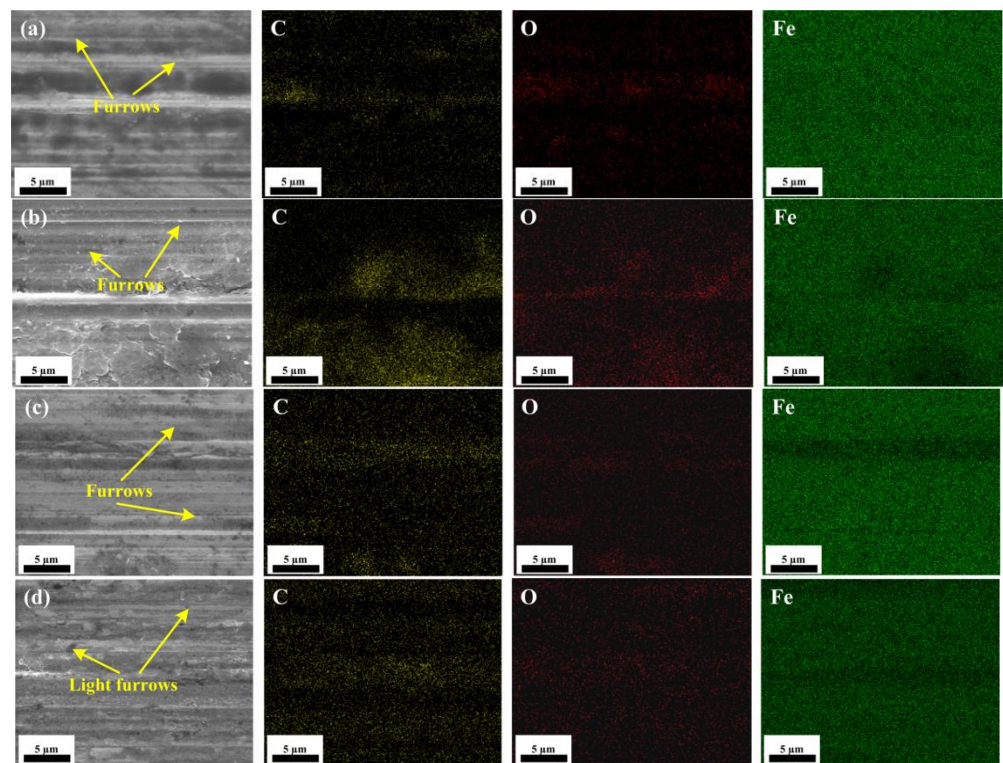
Figure 10. Surface micrographs and EDS elemental maps of wear traces of upper balls after tribological test for the (**a**) water sample, (**b**) GO aqueous sample, (**c**) MBS aqueous sample, and (**d**) MBS–GO aqueous sample (additive content = 0.5 wt%, GO−to−MBS mass ratio = 60:40, load = 10 N, speed = 50 mm/s, and testing time = 30 min).

3.4. Mechanism Analysis

Figure 11 shows the Raman mappings of the wear traces of the lower plates lubricated with water as well as GO, MBS, and MBS–GO aqueous samples (additive content = 0.5 wt%, mass ratio = 60:40, load = 10 N, speed = 50 mm/s, and testing time = 30 min). The change in color indicates the distribution and intensity of the G peak. Substantial wear traces, such as severe scratches, are shown in Figure 11a. The corresponding Raman mapping shows the absence of a G peak on the worn surface lubricated with water. As shown in Figure 11b, the wear traces formed on the lower plate lubricated with the GO aqueous sample are comparatively low. The corresponding Raman mapping of the worn surface detected a broad distribution of G peak, indicating the presence of graphene sheets along the wear trace surface [56]. As shown in Figure 11c, in comparison to Figure 11a, shallower and narrower scratches dominate the worn trace surface lubricated with the MBS aqueous sample. The corresponding Raman mapping of the worn surface showed that the G peak is partially distributed across the wear trace surface, showing that a tribofilm of the MBS nanoparticles has formed within the wear tracks [57]. In Figure 11d, shallower and narrower scratches are visible on the worn trace surface lubricated with the MBS–GO aqueous sample. The corresponding Raman mapping showed that the wide distribution of the G peak is observed throughout the wear surface, which could be attributed to the presence of hybrid nanoparticles in the formed tribofilm. The hybrid nanoparticle tribofilm prevented a direct contact between the two friction surfaces. In addition, the ball-bearing effect of the MBS nanoparticles in the hybrid could help reduce abrasive wear [34,58]. This is consistent with the results shown in Figures 9 and 10.
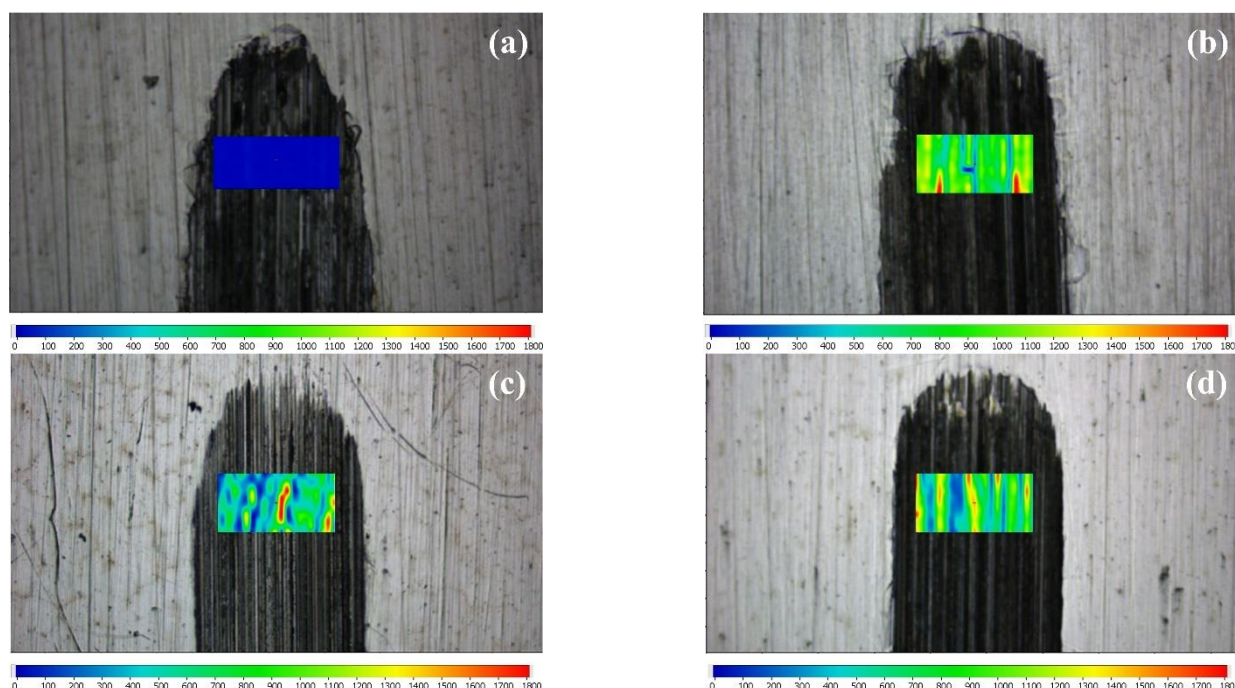
Figure 11. Raman mappings of wear traces of lower plates after tribological test for (**a**) water, (**b**) GO aqueous sample, (**c**) MBS aqueous sample, and (**d**) MBS–GO aqueous sample (additive content = 0.5 wt%, GO−to−MBS mass ratio = 60:40, load = 10 N, speed = 50 mm/s, and testing time = 30 min).

According to the obtained results, the addition of either the GO nanosheets or MBS nanoparticles improved the tribological performance of water. Additionally, when GO nanosheets and MBS nanoparticles were added simultaneously, the lubrication characteristics of water were significantly enhanced. The lubrication mechanisms of the water-based lubricating additive can be summarized as GO nanosheets and MBS nanoparticles showing the characteristic lubricating action of the layered nanoparticles and spherical nanoparticles, respectively [59,60]. As shown in Figure 2, the MBS–GO nanoparticles are hybrid nanoparticles comprising MBS nanoparticles anchored on the GO surface. This type of nanomaterial can deposit on the friction interface, forming a protective tribofilm to effectively prevent a direct contact of the rubbing surfaces. Meanwhile, the MBS nanoparticles in the hybrid nanoparticles provide the lubricating effect by acting as ball bearings [61,62]. As a result, the MBS–GO nanoparticles provide synergistic lubrication effects in water. This suggests that MBS–GO nanoparticles could increase energy savings by improving the lubricating properties of water. In future studies, the wear and the corresponding deposited tribofilm of upper balls lubricated with water containing the MBS–GO nanoparticles should be investigated to further reveal the friction- reduction and antiwear mechanism. Furthermore, the impact of different steel materials of the friction pairs on MBS–GO nanoparticles friction and wear should be investigated systemically, which is crucial for the potential applications of MBS–GO nanoparticles.

4. Conclusions

In this study, the tribological performance of the GO nanosheets, MBS nanoparticles, and MBS–GO nanoparticles as lubricating additives in water was investigated using a ball-on-plate tribometer. The following conclusions can be drawn:

(1)   GO nanosheets have a typical layered structure. When GO nanosheets are used as lubricating additives, a protective graphene tribofilm forms on the rubbing surfaces, improving the tribological properties of water.

(2) MBS nanoparticles have a typical spherical structure. The ball bearing-lubricating effect of the MBS nanoparticles enhances the friction-reduction and antiwear capabilities of water.

(3) In comparison to the GO nanosheets and MBS nanoparticles, water-containing MBS–GO nanoparticles show better lubrication properties. When the additive content is 0.5 wt% and GO−to−MBS mass ratio is 60:40, the friction coefficient and wear volume are reduced by 69.7% and 60.5%, respectively, compared to water. The synergistic effect of the GO nanosheets and MBS nanoparticles during the friction process is primarily responsible for the significant improvement in the lubricating performance of water.

Author Contributions: Conceptualization, C.L., B.W. and X.H.; formal analysis, C.L. and L.L.; funding acquisition, X.C., B.W., X.G. and K.H.; investigation, C.L. and X.W. (Xinyun Wang); methodology, C.L., L.L. and X.W. (Xiaodong Wang); writing—original draft, C.L.; writing—review and editing, X.C., X.W. (Xiaodong Wang), K.H., X.G. and X.H. All authors have read and agreed to the published version of the manuscript.

Institutional Review Board Statement: Not applicable.

Informed Consent Statement: Not applicable.

Data Availability Statement: Not applicable.

Conflicts of Interest: The authors declare no conflict of interest.

References

1. Song, Y.M.; Mandelli, D.; Hod, O.; Urbakh, M.; Ma, M.; Zheng, Q.S. Robust microscale superlubricity in graphite/hexagonal boron nitride layered heterojunctions. *Nat. Mater.* **2018**, *17*, 894–899. [CrossRef] [PubMed]
2. Abdel-Rehim, A.A.; Akl, S.; Elsoudy, S. Investigation of the tribological behavior of mineral lubricant using copper oxide nano additives. *Lubricants* **2021**, *9*, 16. [CrossRef]
3. Sharma, R.V.; Somidi, A.K.; Dalai, A.K. Preparation and properties evaluation of biolubricants derived from canola oil and canola biodiesel. *J. Agric. Food. Chem.* **2015**, *63*, 3235–3242. [CrossRef] [PubMed]
4. Li, Y.Z.; Li, S.W.; Bai, P.P.; Jia, W.P.; Xu, Q.; Meng, Y.G.; Ma, L.R.; Tian, Y. Surface wettability effect on aqueous lubrication: Van der Waals and hydration force competition induced adhesive friction. *J. Colloid Interface Sci.* **2021**, *599*, 667–675. [CrossRef]
5. Rahman, M.H.; Warneke, H.; Webbert, H.; Rodriguez, J.; Austin, E.; Tokunaga, K.; Rajak, D.K.; Menezes, P.L. Water-based lubricants: Development, properties, and performances. *Lubricants* **2021**, *9*, 73. [CrossRef]
6. Morshed, A.; Wu, H.; Jiang, Z. A comprehensive review of water-based nanolubricants. *Lubricants* **2021**, *9*, 89. [CrossRef]
7. Chen, S.Q.; Ding, Q.; Gu, Y.; Quan, X.; Ma, Y.; Jia, Y.L.; Xie, H.M.; Tang, J.Z. Study of tribological properties of fullerenol and nanodiamonds as additives in water-based lubricants for amorphous carbon (a-C) coatings. *Nanomaterials* **2022**, *12*, 139. [CrossRef]
8. Mirzaamiri, R.; Akbarzadeh, S.; Ziaei-Rad, S.; Shin, D.G.; Kim, D.E. Molecular dynamics simulation and experimental investigation of tribological behavior of nanodiamonds in aqueous suspensions. *Tribol. Int.* **2021**, *156*, 106838. [CrossRef]
9. Mou, Z.; Zhao, B.; Wang, B.; Xiao, D. Integration of functionalized polyelectrolytes onto carbon dots for synergistically improving the tribological properties of polyethylene glycol. *ACS Appl. Mat. Interfaces* **2021**, *13*, 8794–8807. [CrossRef]
10. Zhao, J.; Huang, Y.Y.; He, Y.Y.; Shi, Y.J. Nanolubricant additives: A review. *Friction* **2021**, *9*, 891–917. [CrossRef]
11. Fan, K.; Liu, X.K.; Liu, Y.; Li, Y.; Chen, Y.; Meng, Y.Q.; Liu, X.Y.; Feng, W.; Luo, L.B. Covalent functionalization of fluorinated graphene through activation of dormant radicals for water-based lubricants. *Carbon* **2020**, *167*, 826–834. [CrossRef]

12. He, Y.X.; Chen, Q.Y.; Liu, H.; Zhang, L.; Wu, D.Y.; Lu, C.; Yang, W.O.; Jiang, D.F.; Wu, M.F.; Zhang, J.X.; et al. Friction and wear of MoO_3/graphene oxide modified glass fiber reinforced epoxy nanocomposites. *Macromol. Mater. Eng.* **2019**, *304*, 1900166. [CrossRef]

13. Song, H.; Wang, Z.; Yang, J. Tribological properties of graphene oxide and carbon spheres as lubricating additives. *Appl. Phys. A* **2016**, *122*, 933. [CrossRef]

14. Su, F.H.; Chen, G.F.; Huang, P. Lubricating performances of graphene oxide and onion-like carbon as water-based lubricant additives for smooth and sand-blasted steel discs. *Friction* **2020**, *8*, 47–57. [CrossRef]

15. Zhang, G.Q.; Zeng, X.Q.; Ren, T.H.; van der Heide, E. Tribological properties of graphene oxide sheets as water-based lubricant additive. *Ind. Lubr. Tribol.* **2018**, *70*, 1025–1036. [CrossRef]

16. Gan, C.L.; Liang, T.; Li, X.P.; Li, W.; Li, H.; Fan, X.Q.; Zhu, M.H. Ultra-dispersive monolayer graphene oxide as water-based lubricant additive: Preparation, characterization and lubricating mechanisms. *Tribol. Int.* **2021**, *155*, 106768. [CrossRef]

17. Gan, C.L.; Liang, T.; Li, W.; Fan, X.Q.; Li, X.; Li, D.S.; Zhu, M.H. Hydroxyl-terminated ionic liquids functionalized graphene oxide with good dispersion and lubrication function. *Tribol. Int.* **2020**, *148*, 106350. [CrossRef]

18. Min, C.Y.; He, Z.B.; Song, H.J.; Liang, H.Y.; Liu, D.D.; Dong, C.K.; Jia, W. Fluorinated graphene oxide nanosheet: A highly efficient water-based lubricated additive. *Tribol. Int.* **2019**, *140*, 105867. [CrossRef]

19. Wu, D.Y.; Xu, Y.F.; Yao, L.L.; You, T.; Hu, X.G. Tribological behaviour of graphene oxide sheets as lubricating additives in bio-oil. *Ind. Lubr. Tribol.* **2018**, *70*, 1396–1401. [CrossRef]

20. Wu, P.; Chen, X.C.; Zhang, C.H.; Luo, J.B. Synergistic tribological behaviors of graphene oxide and nanodiamond as lubricating additives in water. *Tribol. Int.* **2019**, *132*, 177–184. [CrossRef]

21. Huang, S.Q.; He, A.S.; Yun, J.; Xu, X.F.; Jiang, Z.Y.; Jiao, S.H.; Huang, H. Synergistic tribological performance of a water based lubricant using graphene oxide and alumina hybrid nanoparticles as additives. *Tribol. Int.* **2019**, *135*, 170–180. [CrossRef]

22. Du, S.N.; Sun, J.L.; Wu, P. Preparation, characterization and lubrication performances of graphene oxide-TiO_2 nanofluid in rolling strips. *Carbon* **2018**, *140*, 338–351. [CrossRef]

23. Min, C.Y.; Zhang, Q.Q.; Shen, C.; Liu, D.D.; Shen, X.J.; Song, H.J.; Li, S.J.; Xu, D.; Lin, X.Y.; Zhang, K. Graphene oxide/carboxyl-functionalized multi-walled carbon nanotube hybrids: Powerful additives for water-based lubrication. *RSC Adv.* **2017**, *7*, 32574–32580. [CrossRef]

24. Guo, P.F.; Chen, L.; Wang, J.J.; Geng, Z.R.; Lu, Z.B.; Zhang, G.G. Enhanced tribological performance of aminated nano-silica modified graphene oxide as water-based lubricant additive. *ACS Appl. Nano Mater.* **2018**, *1*, 6444–6453. [CrossRef]

25. Green, D.A.; Lewis, R.; Dwyer-Joyce, R.S. Wear effects and mechanisms of soot-contaminated automotive lubricants. *Proc. Inst. Mech. Eng. Part J J. Eng. Tribol.* **2006**, *220*, 159–169. [CrossRef]

26. Zhang, Q.Q.; Hu, X.G.; Duan, F.Q.; Meng, Y.G. An efficient lubrication approach to mitigate soot-induced wear: Synergistic repair effect of magnetic MoS_2 composites and magnetic field. *Wear* **2022**, *488*, 204182. [CrossRef]

27. Hu, E.Z.; Hu, X.G.; Liu, T.X.; Liu, Y.M.; Song, R.H.; Chen, Y.Z. Investigation of morphology, structure and composition of biomass-oil soot particles. *Appl. Surf. Sci.* **2013**, *270*, 596–603. [CrossRef]

28. Li, C.; Wei, D.Z.; Zhuang, Y.; Song, R.H.; Hu, X.G. Effect of biodiesel soot on the tribological behavior of liquid paraffin. *China Pet. Process. Petrochem. Technol.* **2018**, *20*, 106–113.

29. Mulay, M.R.; Chauhan, A.; Patel, S.; Balakrishnan, V.; Halder, A.; Vaish, R. Candle soot: Journey from a pollutant to a functional material. *Carbon* **2019**, *144*, 684–712. [CrossRef]

30. Liu, T.X.; Wang, J.; Kang, K.; Qin, J.; Tang, Z.Q. Preparation, characterization and tribological properties of coal indirect liquefied diesel soot modified by oleylamine. *Appl. Surf. Sci.* **2021**, *550*, 149351. [CrossRef]

31. Esmeryan, K.D.; Castano, C.E.; Chaushev, T.A.; Mohammadi, R.; Vladkova, T.G. Silver-doped superhydrophobic carbon soot coatings with enhanced wear resistance and anti-microbial performance. *Colloids Surf. A* **2019**, *582*, 123880. [CrossRef]

32. Li, C.; Li, M.L.; Wang, X.Y.; Feng, W.M.; Zhang, Q.Q.; Wu, B.; Hu, X.G. Novel carbon nanoparticles derived from biodiesel soot as lubricant additives. *Nanomaterials* **2019**, *9*, 1115. [CrossRef] [PubMed]

33. Li, C.; Wang, X.Y.; Wu, F.Y.; Liu, T.X.; Hu, X.G. Preparation, characterization and water-based lubricity of modified biodiesel soot. *Chem. J. Chin. Univ.* **2020**, *41*, 987–994.

34. Bondarev, A.V.; Fraile, A.; Polcar, T.; Shtansky, D.V. Mechanisms of friction and wear reduction by h-BN nanosheet and spherical W nanoparticle additives to base oil: Experimental study and molecular dynamics simulation. *Tribol. Int.* **2020**, *151*, 106493. [CrossRef]

35. Fei, J.; Qi, Y.; Luo, L.; Gu, Y.F.; Huang, J.F. Synergistic effect of talc/carbon spheres composite as oil-based additive enhancing the lubricating properties for steel-steel contact. *Lubr. Sci.* **2020**, *32*, 80–89. [CrossRef]

36. Tian, X.; Song, N.N.; Yang, G.B.; Zhou, C.H.; Zhang, S.M.; Zhang, P.Y. Organic-sulfonate functionalized graphene as a high temperature lubricant for efficient antifriction and antiwear in water based drilling fluid. *Tribol. Lett.* **2022**, *70*, 32. [CrossRef]

37. Hao, L.; Hao, W.D.; Li, P.P.; Liu, G.M.; Li, H.Y.; Aljabri, A.; Xie, Z.L. Friction and wear properties of a nanoscale ionic liquid-like GO@ SiO_2 hybrid as a water-based lubricant additive. *Lubricants* **2022**, *10*, 125. [CrossRef]

38. Liu, C.C.; Guo, Y.B.; Wang, D.G. PEI-RGO nanosheets as a nanoadditive for enhancing the tribological properties of water-based lubricants. *Tribol. Int.* **2019**, *140*, 105851. [CrossRef]

39. Li, C.; Hu, X.G. *Biodiesel Soot: Tribology, Properties, and Formation*; Elsevier: Amsterdam, The Netherlands, 2020.

40. Wu, B.; Song, H.; Li, C.; Song, R.H.; Zhang, T.M.; Hu, X.G. Enhanced tribological properties of diesel engine oil with nano-lanthanum hydroxide/reduced graphene oxide composites. *Tribol. Int.* **2020**, *141*, 105951. [CrossRef]

41. Wu, B.; Song, H.; Zhang, Q.Q.; Hu, X.G. Controllable synthesis and friction reduction of $ZnFe_2O_4@C$ microspheres with diverse core-shell architectures. *Tribol. Int.* **2021**, *153*, 106614. [CrossRef]

42. Zhang, Q.Q.; Song, H.; Wu, B.; Feng, W.M.; Li, X.Y.; Jiao, Y.; Hu, X.G. Effect of magnetic field on the tribological behaviors of $Fe_3O_4@ MoS_2$ as polyalphaolefin additive in the steel/steel friction interface. *Wear* **2021**, *466*, 203586. [CrossRef]

43. Wang, J.; Liu, T.X. Study on the Tribological properties of F-T DS/ZnFe-LDH composite lubricating material. *Appl. Sci.* **2022**, *12*, 599. [CrossRef]

44. Zhang, Y.L.; Zhang, R.L.; Rao, L.Z.; Kim, D.C.; Kook, S. The influence of a large methyl ester on in-flame soot particle structures in a small-bore diesel engine. *Fuel* **2017**, *194*, 423–435. [CrossRef]

45. Xu, Y.F.; Geng, J.; Peng, Y.B.; Liu, Z.C.; Yu, J.Y.; Hu, X.G. Lubricating mechanism of $Fe_3O_4@MoS_2$ core-shell nanocomposites as oil additives for steel/steel contact. *Tribol. Int.* **2018**, *121*, 241–251. [CrossRef]

46. Liu, H.L.; Huang, Y.J.; Wang, Y.Z.; Zhao, X.M.; Chen, D.Q.; Chen, G.H. Study of tribological properties and lubrication mechanism of surfactant-coated anthracite sheets used as lubricant additives. *Friction* **2021**, *9*, 524–537. [CrossRef]

47. Li, X.M.; Deng, J.X.; Liu, L.L.; Duan, R.; Ge, D.L. Fabrication of WS_2/C composite coatings via electrohydrodynamic atomization and their tribology behaviours. *Appl. Surf. Sci.* **2021**, *538*, 148128. [CrossRef]

48. Wei, J.X.; Cai, M.R.; Zhou, F.; Liu, W.M. Candle soot as particular lubricant additives. *Tribol. Lett.* **2014**, *53*, 521–531. [CrossRef]

49. Fan, K.; Liu, J.; Wang, X.; Liu, Y.; Lai, W.C.; Gao, S.S.; Qin, J.Q.; Liu, X.Y. Towards enhanced tribological performance as water-based lubricant additive: Selective fluorination of graphene oxide at mild temperature. *J. Colloid Interface Sci.* **2018**, *531*, 138–147. [CrossRef]

50. Wu, B.; Zhang, Q.Q.; Song, H.; Yang, B.X.; Tian, M.; Hu, X.G. Preparation, dispersion and tribological properties of oleophilic lanthanum hydroxide/graphene oxide nanocomposites. *China Pet. Process. Petrochem. Technol.* **2020**, *22*, 111.

51. Zhang, L.L.; Pu, J.B.; Wang, L.P.; Xue, Q.J. Synergistic effect of hybrid carbon nanotube–graphene oxide as nanoadditive enhancing the frictional properties of ionic liquids in high vacuum. *ACS Appl. Mat. Interfaces* **2015**, *7*, 8592–8600. [CrossRef]

52. Tang, J.Z.; Chen, S.Q.; Jia, Y.L.; Ma, Y.; Xie, H.M.; Quan, X.; Ding, Q. Carbon dots as an additive for improving performance in water-based lubricants for amorphous carbon (a-C) coatings. *Carbon* **2020**, *156*, 272–281. [CrossRef]

53. Wang, W.; Dong, S.W.; Gao, Y.; Zhang, G.L.; Wang, K.S. Tribological behaviours of black phosphorus/MoS_2 composites as water-based lubrication additives. *Lubr. Sci.* **2021**, *33*, 404–416. [CrossRef]

54. Hu, Y.W.; Wang, Y.X.; Zeng, Z.X.; Zhao, H.C.; Li, J.L.; Ge, X.W.; Wang, L.P.; Xue, Q.J.; Mao, C.L.; Chen, S.J. BLG-RGO: A novel nanoadditive for water-based lubricant. *Tribol. Int.* **2019**, *135*, 277–286. [CrossRef]

55. Alazemi, A.A.; Etacheri, V.; Dysart, A.D.; Stacke, L.E.; Pol, V.G.; Sadeghi, F. Ultrasmooth submicrometer carbon spheres as lubricant additives for friction and wear reduction. *ACS Appl. Mat. Interfaces* **2015**, *7*, 5514–5521. [CrossRef] [PubMed]

56. Berman, D.; Erdemir, A.; Sumant, A.V. Few layer graphene to reduce wear and friction on sliding steel surfaces. *Carbon* **2013**, *54*, 454–459. [CrossRef]

57. Cai, T.; Zhang, Y.X.; Liu, D.; Tong, D.Y.; Liu, S.G. Nanostructured molybdenum/heteroatom-doped carbon dots nanohybrids for lubrication by direct carbonization route. *Mater. Lett.* **2019**, *250*, 20–24. [CrossRef]

58. Zhang, J.S.; Chen, Z.X.; Wu, H.; Zhao, J.W.; Jiang, Z.Y. Effect of graphene on the tribolayer of aluminum matrix composite during dry sliding wear. *Surf. Coat. Technol.* **2019**, *358*, 907–912. [CrossRef]

59. Uzoma, P.C.; Hu, H.; Khadem, M.; Penkov, O.V. Tribology of 2D nanomaterials: A review. *Coatings* **2020**, *10*, 897. [CrossRef]

60. Ye, M.T.; Cai, T.; Shang, W.J.; Zhao, L.N.; Zhang, Y.X.; Liu, D.; Liu, S.G. Friction-induced transfer of carbon quantum dots on the interface: Microscopic and spectroscopic studies on the role of inorganic–organic hybrid nanoparticles as multifunctional additive for enhanced lubrication. *Tribol. Int.* **2018**, *127*, 557–567. [CrossRef]

61. Zhang, W.L.; Cao, Y.L.; Tian, P.Y.; Guo, F.; Tian, Y.; Zheng, W.; Ji, X.Q.; Liu, J.Q. Soluble, exfoliated two-dimensional nanosheets as excellent aqueous lubricants. *ACS Appl. Mat. Interfaces* **2016**, *8*, 32440–32449. [CrossRef]

62. Guo, P.F.; Qi, S.S.; Chen, L.; Gou, C.X.; Lin, B.; Lu, Z.B.; Wu, Z.G.; Zhang, G.G. Black phosphorus–graphene oxide hybrid nanomaterials toward advanced lubricating properties under water. *Adv. Mater. Interfaces* **2019**, *6*, 1901174. [CrossRef]